



Plate tectonics and mantle controls on plume dynamics

Maëlis Arnould^{a,b,c,d,*}, Nicolas Coltice^a, Nicolas Flament^e, Claire Mallard^c

^a Laboratoire de Géologie, École Normale Supérieure, CNRS UMR 8538, PSL Research University, 24 rue Lhomond, 75005 Paris, France

^b Université de Lyon, École Normale Supérieure de Lyon, Université Claude Bernard, Laboratoire de Géologie de Lyon, Terre, Planètes, Environnement, CNRS UMR 5276, 2 rue Raphaël Dubois, 69622 Villeurbanne, France

^c EarthByte Group, School of Geosciences, The University of Sydney, NSW 2006, Australia

^d Centre for Earth Evolution and Dynamics, Department of Geosciences, University of Oslo, 0371 Oslo, Norway

^e GeoQuEST Research Centre, School of Earth, Atmospheric and Life Sciences, University of Wollongong, Northfields Avenue, Wollongong, NSW 2522, Australia

ARTICLE INFO

Article history:

Received 4 February 2020

Received in revised form 25 May 2020

Accepted 25 June 2020

Available online xxxx

Editor: R. Bendick

Dataset link: <https://osf.io/up7df/>

Keywords:

Mantle plumes
plume drift
numerical modelling
mantle convection
plate-like tectonics

ABSTRACT

Mantle plumes provide valuable information about whole-mantle convection: they originate at the core-mantle boundary, cross Earth's mantle and interact with the lithosphere. For instance, it has been proposed that the mobility/stability of plumes depends on plume intrinsic properties, on how slabs interact with the basal boundary layer, on mantle flow, or on their proximity to mid-ocean ridges.

Here, we use 3D-spherical models of mantle convection generating self-consistent plate-like behaviour to investigate the mechanisms linking tectonics and mantle convection to plume dynamics. Our models produce fully-dynamic mantle plumes that rise vertically with deflection $<10^\circ$ and present excess temperatures, rising speeds, buoyancy and heat fluxes comparable to observations. In the absence of plate tectonics, plumes are stable and their lifetime exceeds hundreds of million years. With plate tectonics, plumes are more mobile, and we identify four physical mechanisms controlling their stability. 1/ Fixed plumes are located at saddle points of basal mantle flow. 2/ Plumes moving at speeds between 0.5–1 cm yr^{-1} are slowly entrained by passive mantle flow. 3/ Fast plume motions between 2–5 cm yr^{-1} lasting several tens of million years are caused by slab push. 4/ Plumes occasionally drift at speeds $>5 \text{ cm yr}^{-1}$ over $<10 \text{ Myr}$ through plume merging. We do not observe systematic anchoring of plumes to mid-oceanic ridges. Independent of the presence of a dense basal layer, plate-like regimes decrease the lifetime of plumes compared to stagnant-lid models. Plume age, temperature excess or buoyancy flux are not diagnostic of plume lateral speed. The fraction of plumes moving by less than 0.5 cm yr^{-1} is $>25\%$, which suggests that fixed hotspot reference frames can be defined from carefully selected hotspot tracks.

© 2020 Elsevier B.V. All rights reserved.

1. Introduction

Since Morgan (1972) linked deep mantle plumes to tectonics motions, combining seismology, petrology and geophysics has led to the characterisation of hotspots and deep mantle plumes. Recent full-waveform tomography suggests that Earth's major plume conduits are vertical and broad, $>600 \text{ km}$ in diameter in the lower mantle, preferentially tilted in the upper mantle and likely anchored at the base of the mantle (French and Romanowicz, 2015). The composition of olivine phenocrysts indicates upper mantle plume excess temperatures between $+150 \text{ K}$ and $+300 \text{ K}$ (e.g. Putirka, 2005). The vertical deflection of oceanic lithosphere by mantle plumes (e.g. Sleep, 1990; Crosby and McKenzie, 2009) and

the propagation velocity of plume-related V-shaped ridges (Poore et al., 2009; Parnell-Turner et al., 2014) constrain plume buoyancy fluxes to between $0.3 \times 10^3 \text{ kg s}^{-1}$ (Bowie, Sleep, 1990) and $>70 \times 10^3 \text{ kg s}^{-1}$ (Iceland, Parnell-Turner et al., 2014). Combining information on plume radius, excess temperature and buoyancy flux gives plume rising speeds between 23 cm yr^{-1} and 54 cm yr^{-1} (Poore et al., 2009; Turcotte and Schubert, 2014) and plume heat flow anomalies between 10–20 mW m^{-2} (Sleep, 1990).

Plumes can provide valuable information about the physics of mantle convection since they potentially interact with the whole mantle, including both the basal and top boundary layer. Several studies have focused on characterising the temporal stability of mantle plumes, because fixed plumes can serve as an absolute reference for global tectonic reconstructions (e.g. Wilson, 1963). However, paleomagnetic, geochronological and petrological studies suggest contrasting plume stability/mobility. Early geochronological and paleomagnetic observations (e.g. Morgan, 1981), and studies of the uncertainties of plate-reconstruction circuits (e.g. Duncan,

* Corresponding author now at Centre for Earth Evolution and Dynamics, Department of Geosciences, University of Oslo, 0371 Oslo, Norway.

E-mail address: maelis.arnould@geo.uio.no (M. Arnould).

Table 1
Non-dimensional and dimensional model parameters.

Parameter	Non-dim. value	Dim. value
Surface temperature (T_{top})	0.12	255 K
Basal temperature (T_{bot})	1.12	2240–2645 K
Mantle thickness (D)	1	2890 km
Reference thermal expansivity (α_0)	1	$3 \times 10^{-5} \text{ K}^{-1}$
Reference density (ρ_0)	1	4400 kg m $^{-3}$
Reference diffusivity (κ_0)	1	$1 \times 10^{-6} \text{ m}^2 \text{ s}^{-1}$
Reference heat capacity (c_{p0})	1	715 J kg $^{-1} \text{ K}^{-1}$
Reference viscosity (η_0)	1	$1 \times 10^{22} \text{ Pa s}$
Internal heating rate (H)	40–50	$7.54\text{--}9.43 \times 10^{-12} \text{ W kg}^{-1}$
Activation energy (E_a)	8	142 kJ mol $^{-1}$
Activation volume (V_a)	3	0.44 cm 3 mol $^{-1}$
Maximum viscosity cut-off	10^4	10^{26} Pa s
Viscosity factor below 660 km depth	30	
Yield stress gradient for all materials ($d\sigma_Y$)	2.34×10^6	1088 Pa m $^{-1}$
Oceanic lithosphere surface yield stress ($\sigma_{Y0,oc}$)	$2\text{--}200 \times 10^4$	27–270 MPa
Weak-crust surface yield stress (Model 5, $\sigma_{Y0,wc}$)	1×10^4	13 MPa
Weak-crust thickness (Model 5)	0.005	14 km
Continental interior surface yield stress ($\sigma_{Y0,cont}$)	7×10^5	932 MPa
Continental interior viscosity factor	100	
Continental interior buoyancy number (B_{cont})	−0.32	−150 kg m $^{-3}$
Continental interior thickness	0.0692	200 km
Continental belt surface yield stress (σ_{Ybelt})	3×10^5	400 MPa
Continental belt viscosity factor	50	
Continental belt buoyancy number (B_{belt})	−0.4	−188 kg m $^{-3}$
Continental belt thickness	0.0432	125 km
Basal thermochemical layer buoyancy number (B_{llsvp})	0.25	117 kg m $^{-3}$ (2.7%)
Basal thermochemical layer initial thickness	0.17	500 km
Basal thermochemical layer viscosity factor	10	

1981) suggested negligible Indo-Atlantic plume motions during the last 100 Myr. In contrast, more recent analyses of geochronological and paleomagnetic datasets suggested either a true polar wander episode (e.g. Koivisto et al., 2014), a change in Pacific plate motion (e.g. Torsvik et al., 2017), a southward motion of the Hawaiian plume reaching 4 cm yr $^{-1}$ between 81 and 47 Ma (e.g. Tarduno et al., 2003), or a combination of plume and plate motion (e.g. Finlayson et al., 2018; Konrad et al., 2018) to explain the bent Hawaii-Emperor hotspot track. Petrological data also suggest that the Azores plume has drifted northwards by 1–2 cm yr $^{-1}$ along the Mid-Atlantic ridge over the last 85 Myr (Arnould et al., 2019).

Numerical and laboratory experiments give independent constraints on mantle plume behaviour. The viscosity contrast between plume conduits and the ambient mantle (e.g. Jellinek and Manga, 2004) may influence their dynamics and stability. Mantle convection has also been shown to contribute to plume motion. A highly viscous lower mantle (Richards, 1991) or the anchoring of plume conduits along the edges of dense basal thermochemical heterogeneities (e.g. Davaille et al., 2002) representing Large Low Shear Velocity Provinces (LLSVPs), is expected to stabilise plumes, while lateral mantle flow, sometimes called *mantle wind* (Duncan and Richards, 1991; Richards and Griffiths, 1988), would favour highly tilted plumes (Steinberger and O’Connell, 1998; O’Neill et al., 2005). Finally, plate tectonics have been proposed to promote plume stability via ridge capture (e.g. Tarduno et al., 2009). Subduction can also indirectly induce plume motions through the effect of supercontinent cycles on the planform of global convection (Zhong et al., 2007) or the lateral push of plume conduits by lower mantle slabs (Hassan et al., 2016).

Collectively, the above-mentioned studies highlight the need to investigate the coupled behaviour of mantle plumes, plate tectonics, large-scale mantle flow and basal thermochemical structures. Here we use time-dependent 3D-spherical numerical models of whole-mantle convection at Earth-like convective vigour and self-generating plate tectonics to jointly investigate the mechanisms linking plate tectonics, mantle convection and plume dynamics. In these models, drifting plumes arise self-consistently and dynamically interact with surface tectonics, large-scale and small-scale

convection. Focusing on model plume conduits, we show that their number, lifetime, shape, temperature excess, rising speed, buoyancy and heat fluxes are comparable to observations. This serves as a basis to investigate the role of plate tectonics, plate layout, convective vigour of the lowermost mantle and basal thermochemical structures on plume spatio-temporal dynamics.

2. Methods

2.1. Numerical models of mantle convection with plate-like tectonics

We solve the conservation equations of mass, momentum, energy and composition under the Boussinesq approximation to produce a series of 3D-spherical models of mantle convection with plate-like tectonics using the code StagYY (Tackley, 2008).

The reference Rayleigh number Ra_0 used to model Earth-like mantle convective vigour is

$$Ra_0 = \frac{\alpha_0 \rho_0 g \Delta T D^3}{\kappa_0 \eta_0} = 10^7 \quad (1)$$

with α_0 the surface thermal expansivity, ρ_0 the reference density, g the gravitational acceleration, ΔT the temperature difference across the mantle domain, D the mantle domain thickness, η_0 the reference viscosity and κ_0 the reference thermal diffusivity. All parameters are listed in Table 1.

Viscosity varies both radially and laterally, and depends on both temperature and pressure as:

$$\eta(T, z) = \eta_0(z) \exp \left(A + \frac{E_a + \Pi(z)V_a}{RT} \right) \quad (2)$$

with A chosen *a priori* so that $\eta = \eta_0$ when $T = 0.64$ (dimensional equivalent 1,600 K) at the lithosphere-asthenosphere boundary, E_a the activation energy, V_a the activation volume, $\Pi(z)$ the static pressure, R the gas constant, z the depth and T the temperature. The activation energy and volume used in the models produce seven orders of magnitude of viscosity variation throughout the

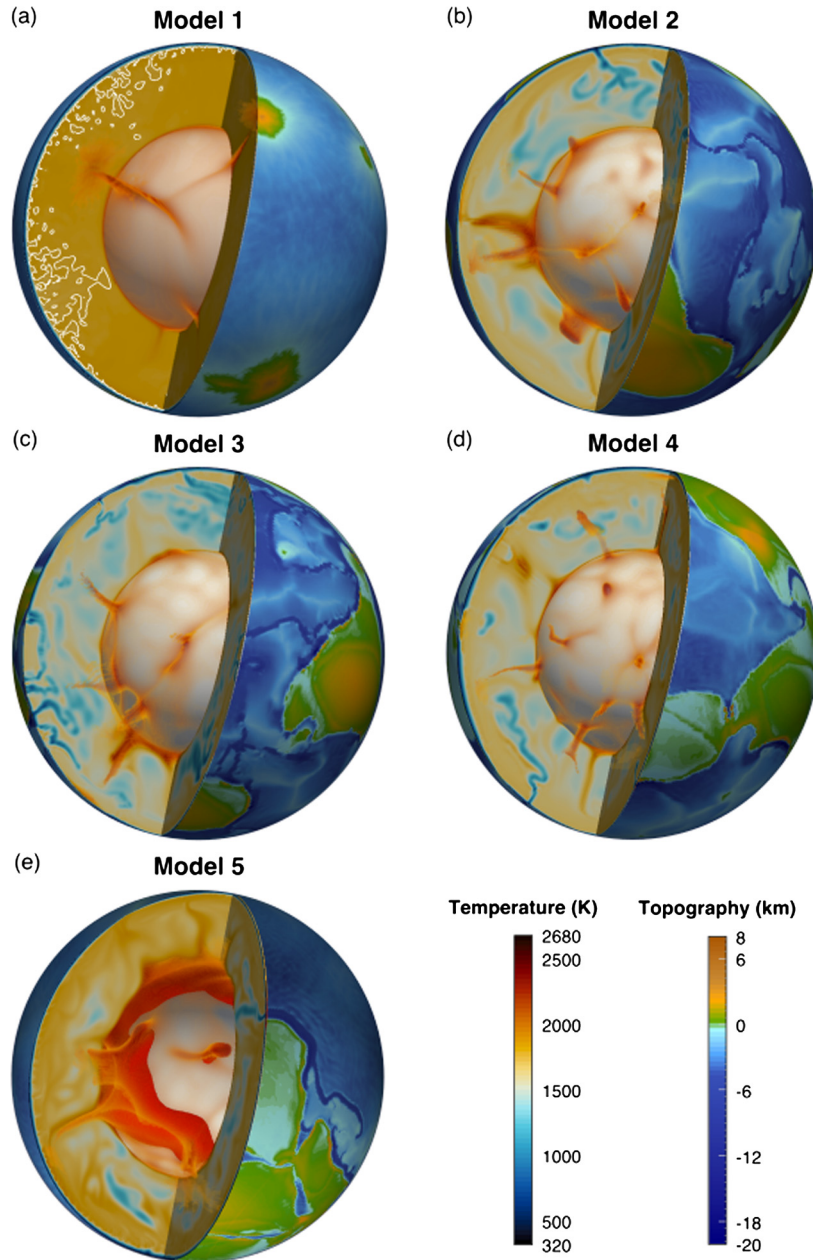


Fig. 1. 3D snapshots of (a) Model 1, (b) Model 2, (c) Model 3, (d) Model 4 and (e) Model 5. Temperature is shown in the interior of the shells and topography at their surface. The white isotherm on (a) highlights small-scale convection. The red isotherm on (e) delineates basal thermochemical heterogeneities. (For interpretation of the colours in the figure(s), the reader is referred to the web version of this article.)

domain (Fig. S1). We impose a viscosity increase by a factor of 30 at 660 km depth, consistent with geoid and postglacial rebound studies (Nakiboglu and Lambeck, 1980; Ricard et al., 1993). Although it remains debated (e.g. Rudolph et al., 2015), the chosen viscosity structure is comparable to most numerical studies (e.g. Steinberger and Calderwood, 2006). In order to achieve self-generation of a plate-like behaviour, we use a pseudo-plastic rheology in which viscosity depends on the yield stress (Tackley, 1998):

$$\eta_Y = \frac{\sigma_Y}{2\dot{\epsilon}_{II}} \quad (3)$$

with η_Y the yielded viscosity, $\sigma_Y = \sigma_{Y_0} + z \times d\sigma_Y$ the yield stress where σ_{Y_0} is the yield stress at the surface and $d\sigma_Y$ is its depth-dependence. $\dot{\epsilon}_{II} = \sqrt{0.5\dot{\epsilon}_{ij}\dot{\epsilon}_{ij}}$ is the second invariant of the strain rate.

We consider five models to investigate the effect of mantle and subduction dynamics on mantle plumes characteristics and drift (Fig. 1, Table 2). In Model 1 (no yielding), we test the effect of a stagnant lid on plume stability. This model does not contain continents, contrary to Models 2-5. The surface yield stress of oceanic lithosphere is equal to 48 MPa and to 27 MPa in Models 2 and 3, respectively. These yield stress values are within the range of those determined from earthquake stress release (Allmann and Schearer, 2009) and from rock mechanics experiments (e.g. Brace and Kohlstedt, 1980), although caution is required when comparing values inferred from mechanisms occurring at different spatial and temporal scales. They result in a mobile plate-like regime with slow (Model 3) or fast (Model 2) plate motions. In Models 1-3 thermal expansivity decreases with depth by a factor of three, to account for less vigorous convection in the lowermost mantle (Chopelas and Boehler, 1992). In Model 4 the surface yield stress is the same

Table 2

Key model parameters for all models (w.c. = weak crust, depth dep. = depth-dependent thermal expansivity, Continents = ages of initial continental configuration). Average plateness and surface mobility of all models. Modelled average and standard deviation of surface (\mathbf{v}_{rms}), mantle horizontal (\mathbf{v}_m), mantle net rotation (NR) and plume absolute (\mathbf{v}_{ha}) and relative (\mathbf{v}_{hr}) velocities in the upper (UM, between 150 and 410 km depth) and the lower (LM, between 670 km depth and the CMB) mantle. Mobility and plateness are dimensionless.

Parameter	Model 1	Model 2	Model 3	Model 4	Model 5	Dobrovine et al. (2012)	Tetley et al. (2019)
Yield stress (MPa)	no yielding	48	27	48	61 (w.c.)		
Thermal expansivity	depth dep.	depth dep.	depth dep.	constant	depth dep.		
LLSVPs	no	no	no	no	yes		
Continents	no	80 Ma	80 Ma	80 Ma	200 Ma		
Plateness		0.90	0.77	0.84	0.87		
Mobility		1.29	1.69	1.62	1.60		
Surface \mathbf{v}_{rms} (cm/yr)	0.002	2.90 ± 0.85	3.32 ± 0.22	3.79 ± 0.60	5.04 ± 1.83	2 – 6	1.5 – 4.8
Mean UM \mathbf{v}_m (cm/yr)	2.34 ± 0.82	3.19 ± 0.57	2.77 ± 0.32	3.60 ± 0.57	4.85 ± 1.52		
Mean LM \mathbf{v}_m (cm/yr)	0.85 ± 0.25	0.91 ± 0.26	0.74 ± 0.15	1.01 ± 0.23	1.23 ± 0.35		
Average NR ($^\circ$ /Myr)	0.001 ± 0.0003	0.039 ± 0.014	0.031 ± 0.013	0.039 ± 0.016	0.029 ± 0.009	0.13 – 0.53	0.05 – 0.11
Mean UM \mathbf{v}_{ha} (cm/yr)	0.57 ± 0.45	1.80 ± 1.13	1.74 ± 0.78	2.22 ± 0.82	2.40 ± 0.77	1.12 ± 0.31	2.07 ± 0.80
Mean UM \mathbf{v}_{hr} (cm/yr)	0.63 ± 0.64	1.55 ± 1.58	1.61 ± 1.18	2.20 ± 1.28	2.22 ± 1.15	0.87 ± 0.35	1.46 ± 1.07
Mean LM \mathbf{v}_{ha} (cm/yr)	0.39 ± 0.51	1.32 ± 0.56	1.05 ± 0.32	1.79 ± 0.90	2.04 ± 1.25		
Mean LM \mathbf{v}_{hr} (cm/yr)	0.44 ± 0.68	1.02 ± 0.83	0.77 ± 0.47	1.66 ± 1.37	2.01 ± 1.90		

as in Model 2 but thermal expansivity is constant with depth, to test the effect of a more vigorous lowermost convection on plume drift. In Model 5, thermal expansivity varies with depth, the surface oceanic lithosphere yield stress is equal to 61 MPa and an uppermost weak-crust layer of 14 km with a yield stress equal to 13 MPa favours the formation of asymmetric subduction (Crameri et al., 2012). Model 5 is the last model of Coltice et al. (2019) for the period 555 to 905 Myr. It includes two basal chemical heterogeneities that are about 3% denser and 10 times more viscous than the ambient mantle, initially 500 km thick and laterally homogeneous with a configuration comparable to present-day LLSVPs (see Fig. S3 of Coltice et al. (2019)). In Models 2–5, the yield-stress slightly increases with depth (Table 2). In Models 2, 3 and 4, the average radial resolution is 31 km while it is 23 km in Model 1 and 5; it is less than 15 km and 10 km near the surface and the core-mantle boundary respectively. The horizontal resolution at the surface varies between 26 km (Models 1 and 5) and 35 km (Models 2–4).

We track the evolution of compositional fields using the tracer-ratio method (Tackley and King, 2003). Model continents are low-density lithospheric rafts, thicker and stiffer than the oceanic lithosphere to prevent their entrainment by the convective flow (Table 1). Despite these characteristics, their margins are recycled through time (Supplementary Movies 1–3), consistent with estimates of continental recycling at subduction zones (Coltice et al., 2019). Their initial shapes correspond to continents reconstructed either 80 Ma ago (separated, Models 2–4, Fig. S2c) or 200 Ma ago (aggregated, Model 5 Coltice et al. (2019)). In Models 1–4, after a preliminary equilibration phase of approximately 200 Myr during which tracers are not advected, we allow continents to dynamically interact within the convective environment for at least 200 Myr. We then analyse mantle plume behaviour over a subsequent period of approximately 350 Myr.

The use of pseudo-plasticity favours Earth-like surface velocities and tectonics (e.g. Coltice et al., 2017). As in Arnould et al. (2018), we verify that Models 2–5 favour plate-like behaviour with Earth-like plateness (proxy for the degree of surface deformation localisation, Tackley, 2000), surface mobility, plate velocities, heat flow and topography (Table 2, Fig. 1, Fig. S3(a), Movies S1 and S2).

2.2. Automated detection of mantle plumes

We developed a plume detection scheme to track plume positions and characteristics through time in map view. We located mantle plume conduits in the upper mantle (at 250, 350 and 670 km depth) and in the lower mantle (at 1,000 km depth) from

their anomalously large radial heat advection, which is proportional to $v_z T$ (with v_z the radial velocity and T the temperature, Fig. S3b). Plumes were defined by upper and lower mantle heat advection equal to 190 K myr^{-1} (Fig. S4) and 48 K myr^{-1} respectively. The greater upper mantle threshold value reflects greater rising speeds. The use of the temperature (e.g. Labrosse, 2002) or radial velocity field alone (e.g. Hassan et al., 2015) is not selective enough to detect mantle plumes in our models. We chose a unique threshold at each depth to directly compare different models (Fig. S4). Results were verified visually for artifacts that could be introduced by the use of threshold values.

We used the connectivity method described in Labrosse (2002) in order to identify distinct plume conduits. We assigned identities (IDs) to plume conduits, and we inferred their location from their geometrical centroid. We tracked plumes in 1 Myr intervals by connecting plumes located within a radius of 500 km with a method similar to that of Hassan et al. (2015), although with a larger radius to follow plumes moving at several tens of cm yr^{-1} . We used this plume tracking method to recover plume positions and characteristics in the upper and the lower mantle over time.

We used *pyGPlates* (Muller et al., 2018) to extract the time-dependent motion of each mantle plume conduit. We calculated absolute model plume velocities averaged over 5 Myr to eliminate artificial plume wobbling caused by rapid readjustments of plume conduit shape. We calculated the relative motions of all plumes with respect to one another at 5 Myr intervals to compare them to observations.

Using StagYY, net rotation is zero at the surface. Therefore, in our models, “net rotation” is the net rotation of the mantle with respect to a fixed surface.

3. Phenomenology of model mantle plumes

We first describe and quantify the spatio-temporal characteristics of model mantle plumes. The goal is to compare them to those deduced from observations to assess the applicability of our models to Earth.

3.1. Number

On average, we detected between 15 (Models 1 and 5) and 35 upper mantle plumes (Model 4) (Fig. 2a). The number of plumes remains relatively stable over the considered timescale. However, longer model evolutions suggest that supercontinent cycles influence the number of active plumes (Coltice et al., 2019). The number of mantle plumes increases with plate-like behaviour (Models

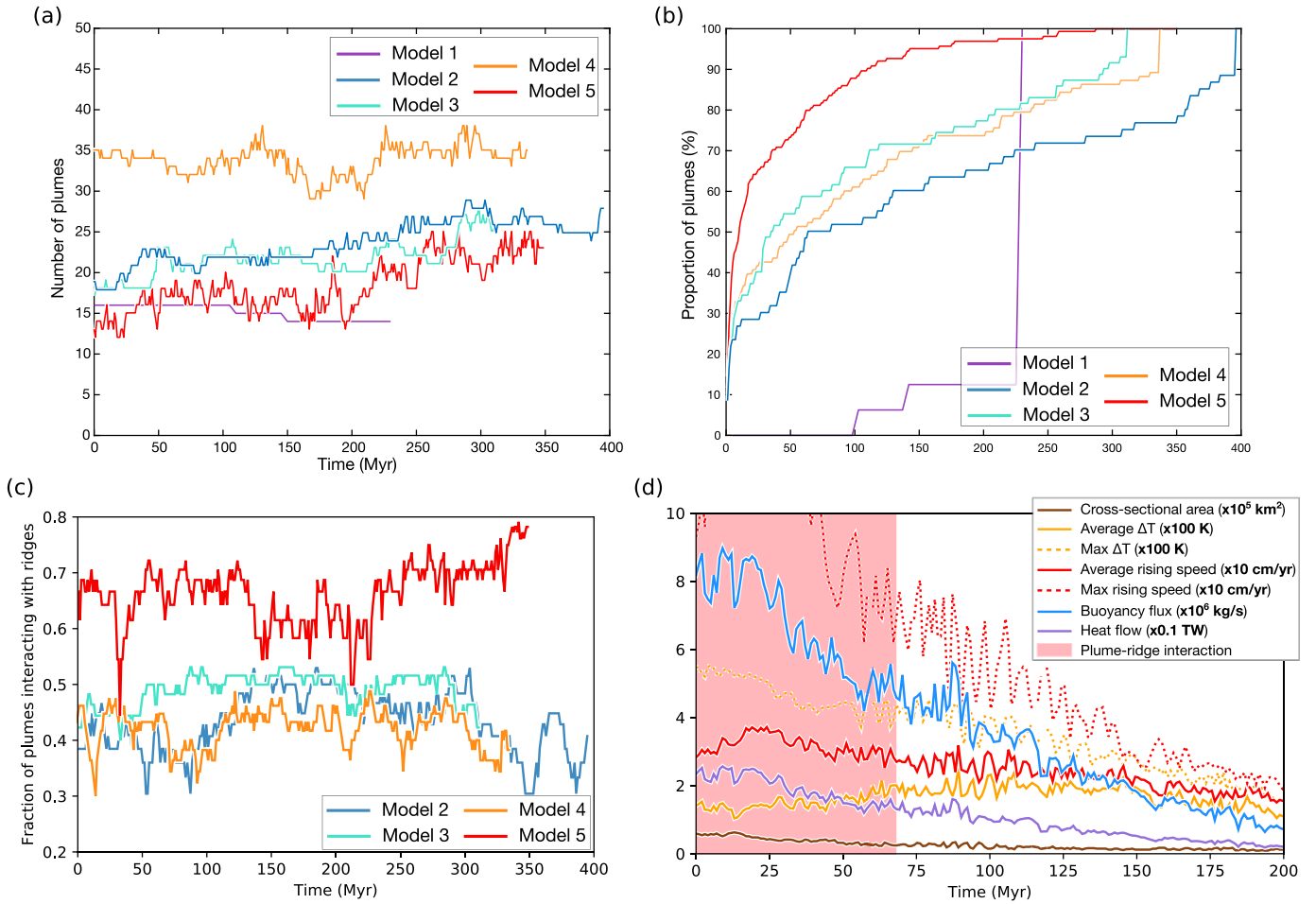


Fig. 2. Evolution, at 350 km depth, of (a) the number of plumes, (b) the cumulative lifetime of plumes and (c) the fraction of plumes interacting with ridges. (d) Temporal evolution of plume characteristics for Plume ID 6 in Model 2 (Fig. S3(a) and (b)): cross-sectional area (brown), average (orange) and maximum (orange, dashed) temperature excess, average (red) and maximum (red, dashed) buoyant rising speed, buoyancy flux (blue) and heat flux (purple). The units of each curve is listed in the figure key. The duration of plume-ridge interaction is highlighted by the pink area. (For interpretation of the colours in the figure(s), the reader is referred to the web version of this article.)

2 and 3 versus Model 1) and with increasing core mantle boundary (CMB) heat flow. Indeed, the 15% larger CMB heat flow due to more vigorous lower mantle convection in Model 4 (Fig. 3f) leads to approximately 30% more plumes than in Model 2 (Fig. 2a) while the presence of a basal thermochemical layer in Model 5 results in a CMB heat flow half that of Model 2 (Fig. 3f), and in a smaller number of plumes than in Model 2 (Fig. 2a).

The number of detected plumes is in broad agreement with other numerical models of whole-mantle convection although model parameters (including physical assumptions and surface boundary conditions) differ (e.g. Davies and Davies, 2009; Hassan et al., 2015; Li and Zhong, 2019). On Earth, the number of hotspots of lower mantle origin remains debated. Courtillot et al. (2003) used strict criteria to propose that only seven hotspots have a deep origin. Doubrovine et al. (2012) used only five deep mantle plumes to constrain absolute plate motions. Wang et al. (2018) proposed 24 deep-rooted mantle plumes from criteria less strict than Courtillot et al. (2003).

3.2. Lifetime

In Models 2-4, 30% of detected plumes persist for at least 200 Myr (Fig. 2b). In Model 1, all but one mantle plumes exist throughout the model evolution, suggesting that the absence of plate-like tectonics leads to long-lived mantle plumes. In contrast, the lifetime of almost all plumes in Model 5 is shorter than 150 Myr (Fig. 2b), potentially because the deformation of basal ther-

mochemical structures by slabs perturbs the buoyancy field that triggers and sustains mantle plumes (Heyn et al., 2018).

These results are compatible with the longest lived oceanic hotspot tracks for St-Helena (about 120 Myr), Tristan (about 120 Myr) and New England (about 130 Ma) plumes (Duncan, 1984; Williams et al., 2015). Shorter-lived hotspot tracks (e.g. Hawaii and Louisville active at least from 87 Ma) terminate at subduction zones, but may have been active longer, the potential oldest parts of their tracks having been subducted (e.g. Portnyagin et al., 2008). Finally, geochemical analyses suggest that South Pacific Cook-Austral plumes have been active for at least 120 Ma (e.g. Konter et al., 2008).

3.3. Shape and radius

In all models, large plume heads initiate in the lowermost mantle and reach the uppermost mantle (Movies S1 and S2). Most plumes consist of one individual conduit (Fig. 1). Some distinct upper mantle plume conduits are merged in the lower mantle (Fig. S8 and Movie S3). This is consistent with seismic tomography models that suggest a connection of Ascension and St-Helena plumes below the transition zone (Montelli et al., 2006), of the Azores, the Canaries and Cape-Verde below 1,400 km depth and of Kerguelen and Crozet below 2,300 km depth (Davaille and Vatteville, 2005).

We quantified mantle plume tilt angle to investigate the possible effect of lateral mantle flow on their motions (Richards and Griffiths, 1988). Model plume conduits are generally vertical: the

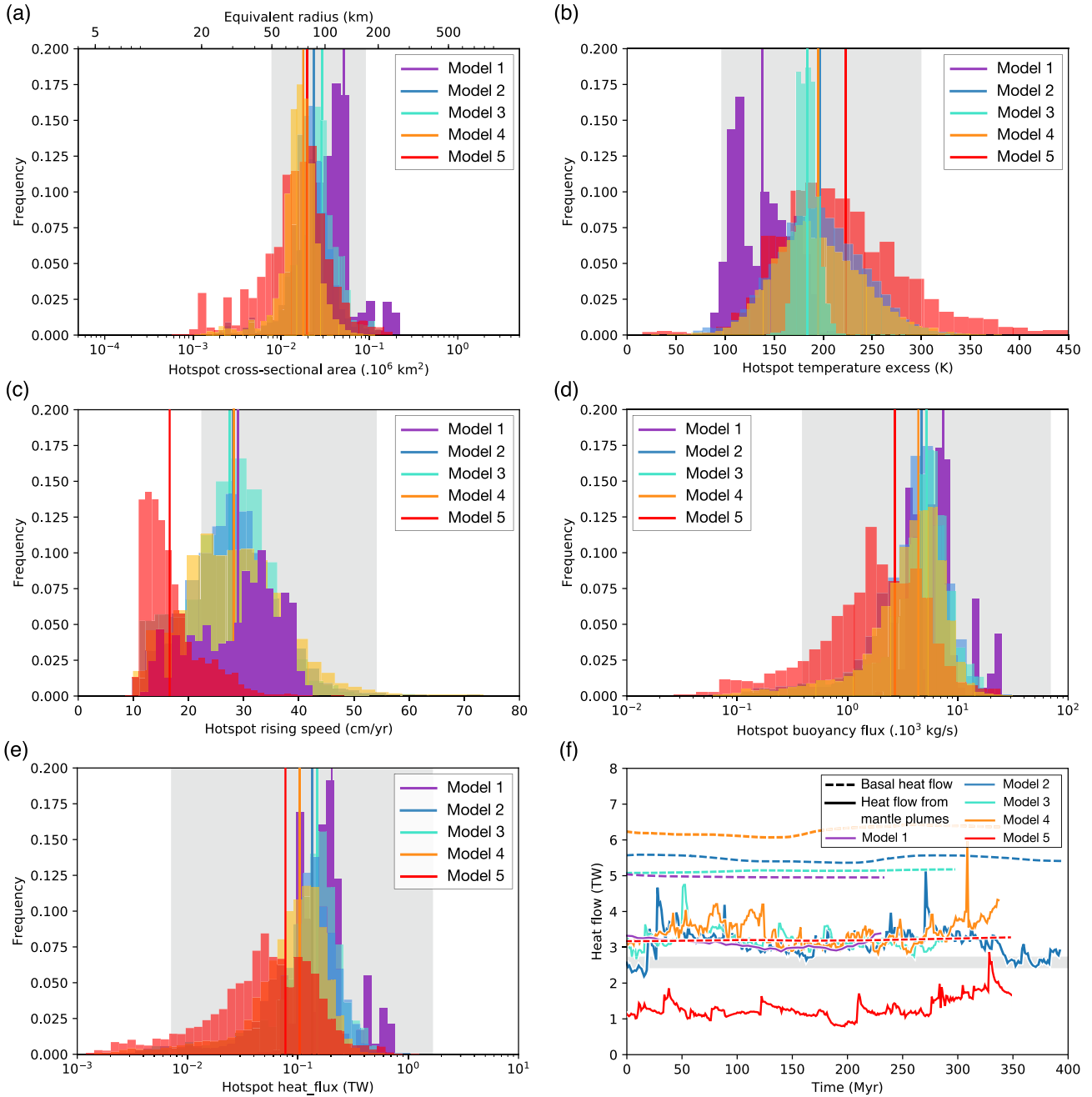


Fig. 3. Distribution of (a) the radius, (b) the excess temperature, (c) the buoyant rising speed, (d) the buoyancy flux and (e) the heat flow of mantle plumes for all models at 350 km depth. Temporal evolution of (f) the core and plume heat flow in all models at 350 km depth. Spikes in plume heat flow correspond to the occasional birth of highly-vigorous plumes. The grey areas highlight the range of observational values for each plume characteristic (see text for details).

average tilt angle between 1,000 km depth and 350 km depth is approximately 5.5° in Models 1–4 (Fig. 4a) and 16.5° in Model 5. In all models, only a limited proportion of plume conduits is deflected by more than 10° ; tilt angles rarely reach the 60° maximum used in plume-particle backward advection models (e.g. Steinberger and O’Connell, 2000). Mantle plume conduits are more likely deflected in the upper mantle than in the lower mantle, consistently with seismic tomography (French and Romanowicz, 2015): in Model 2, the upper-mantle average tilt angle is equal to 15° , compared to 28° in Model 5 (Fig. 4b), due to upper mantle shearing by surface plates, which can also cause deformation of the thermal trail of plumes (Fig. 4b).

The average upper mantle plume radius varies from 130 km for stagnant-lid convection (Model 1) to 75 km for vigorous

lower mantle convection (Model 4). Buoyancy fluxes deduced from hotspot topographic swells (Sleep, 1990) indicate that the average radius of upper mantle plume conduits is of the order of 100 km. This radius is small compared to seismic tomography resolution, which explains the difficulties in imaging plume conduits.

The radius of plume conduits is systematically greater in the lower mantle than in the upper mantle (377 km in Model 1 at 1,000 km depth to 131 km in Model 4, Fig. 1 and S6a). The difference in plume conduit radius between the lower and upper mantle is due to the 30 fold viscosity jump imposed at 670 km depth (e.g. Leng and Gurnis, 2012). The presence of thermochemical heterogeneities within plumes (Davaille and Vatteville, 2005) and the visco-plastic rheology of the lower mantle (Davaille et al., 2018)

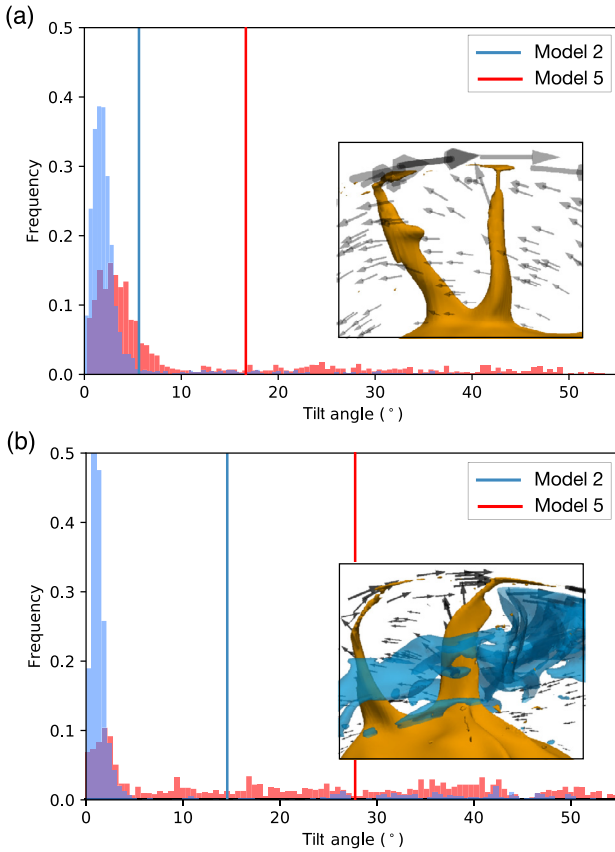


Fig. 4. (a) Upper-lower mantle (350–1000 km depth) and (b) upper mantle (150–670 km depth) plume tilt angle distribution for Models 2 and 5. The average tilt angle is shown as a vertical line. Insets show (a) near vertical and (b) tilted conduits (orange isotherm) in Model 5. Transparent black arrows show the direction of mantle flow. In (b) mantle flow deflects plume conduits in the vicinity of subducting lithosphere (transparent blue isotherm). Note that plume deflection mainly occurs in the uppermost mantle.

might partly explain why lower mantle plumes are broader in tomography models (French and Romanowicz, 2015).

In Model 5, all plumes but one are anchored to basal thermochemical heterogeneities (about 120 different hotspots were detected over 350 Myr). Plumes originate from topographic crests (Fig. 1), either along the edges or on the top of the basal thermochemical heterogeneities, as in previous models that consider dense and hot basal material (Garnero and McNamara, 2008; Hassan et al., 2015; Li and Zhong, 2017, 2019).

3.4. Excess temperature

Model plume average excess temperature is defined as the difference between the average temperature over their cross-sectional area and the average mantle temperature at 350 km depth. The average excess temperature of model plume conduits over their cross-sectional area is +140 K in Model 1 and +200–225 K in Models 2–5 (Fig. 3b), which is consistent with petrological studies (e.g. Putirka, 2005). The lower excess temperature in Model 1 results from the stagnant-lid regime leading to a larger ambient mantle temperature in this model. The average excess temperature decreases with depth along plume conduits (Fig. S6b): it is for example 450 K in average for Model 2 at 1000 km depth.

3.5. Buoyant rising speed

In Models 1–4 (thermal plumes only), plume material rises in the upper mantle at approximately 30 cm yr^{−1} on average (Fig. 3c).

The average rising speed is consistent with the modified Stokes velocity (Richards and Griffiths, 1988):

$$v_p = \frac{k_p \Delta \rho g r_p^2}{\eta} \approx 24 \text{ cm yr}^{-1} \quad (4)$$

with $\eta \approx 1 \times 10^{20}$ Pa s the viscosity of the upper mantle in our models (Fig. S1), $k_p \approx 0.54$ a geometrical constant determined experimentally, $\Delta \rho = \alpha \rho_m \Delta T \approx 22 \text{ kg m}^{-3}$ the density contrast between thermal plumes and the surrounding upper mantle (where $\Delta T \approx 200$ K, α is the thermal expansivity and ρ_m is the reference density), g the gravitational acceleration and $r_p \approx 80$ km the plume radius.

In Model 5 (thermochemical plumes), buoyant rising upper mantle speeds are only approximately 17 cm yr^{−1} because entrained denser basal material decreases the positive thermal buoyancy of plume material.

3.6. Buoyancy flux

We calculated the buoyancy flux of mantle plumes as in Sleep (1990) (Fig. 3d):

$$B_p = \rho_m \alpha \Delta T A_p v_p \quad (5)$$

with ρ_m the reference mantle density, α the reference thermal expansivity, ΔT the mantle plume temperature excess, A_p the cross-sectional area of mantle plume conduits and v_p the buoyant rising speed. In Models 2–4, plume buoyancy flux ranges between 0.01 and $20 \times 10^3 \text{ kg s}^{-1}$ and is $\sim 5 \times 10^3 \text{ kg s}^{-1}$ on average. In Model 1, it is $8 \times 10^3 \text{ kg s}^{-1}$ on average because of the larger cross-sectional area of mantle plumes, and in Model 5 it is $2.5 \times 10^3 \text{ kg s}^{-1}$ because of the lower plume rising speed. This range of model plume buoyancy fluxes is comparable to estimates for present-day hotspots (Crosby and McKenzie, 2009).

3.7. Heat flow

Plume heat flow was derived from the buoyancy flux as in Sleep (1990):

$$F_p = B_p \frac{c_p}{\alpha} \quad (6)$$

where c_p is the mantle heat capacity in J kg^{−1} K^{−1}. Individual plumes advect about 0.08–0.23 TW of heat on average in Models 1–5 (Fig. 3e). In Models 1–5, the core heat flow varies between 3 TW (Models 5) and 6.3 TW (Model 4, Fig. 3f), and never exceeds 20% of the surface heat flow (Fig. S5), which is at the lowest end of observational constraints (5–15 TW, Lay et al., 2008). The amount of heat carried by mantle plumes at 350 km depth represents ~ 3 TW in Models 1–4 and ~ 1.5 TW in Model 5, about 2 TW less than the corresponding heat flow (Fig. 3f). Davies (1988) and Sleep (1990) estimated the contribution of plumes to the total surface heat flow as 2.5 TW from hotspot swells. At 350 km depth, model mantle plumes carry a similar amount of heat. The ratio of upper-mantle plume heat flow to core heat flow (about 50–60% in Models 1–5) is consistent with numerical models of incompressible and isoviscous (Labrosse, 2002) or temperature-dependent viscosity convection with different internal heating rates (Mittelstaedt and Tackley, 2006).

The amount of heat carried by each plume is about 1.5 times larger at 1000 km depth than at 350 km depth (Fig. S6). Mittelstaedt and Tackley (2006) showed that plumes contribute to heat up sinking slabs, therefore losing some heat on their way up (Fig. S6). Using extended-Boussinesq (Leng and Zhong, 2008; Zhong, 2006) and compressible models (Bunge, 2005), it was also suggested that the proportion of core heat flux advected by plumes

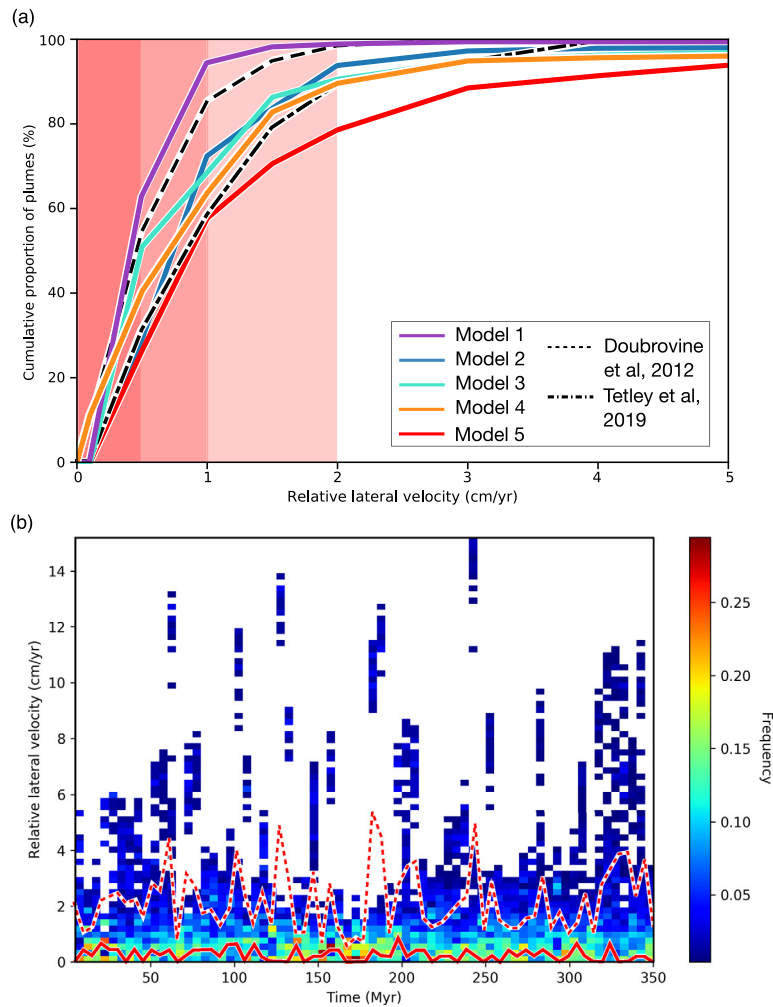


Fig. 5. (a) Time-averaged cumulative distribution of relative plume velocities in all models and as estimated for Earth by Doubrovine et al. (2012) and OptAPM1-M16 of Tetley et al. (2019). The transparent red background rectangles highlight the cumulative proportion of plumes moving at less than 0.5, 1 and 2 cm yr^{-1} . (b) Density plot of the temporal evolution of upper mantle RMS pair-wise lateral relative velocity distribution between mantle plumes in Model 5. Relative velocities are calculated in 5 Myr intervals. The thick red line is the temporal evolution of the mode of relative mantle plume velocities. The dashed red line is the temporal evolution of the average relative velocities between mantle plumes. (For interpretation of the colours in the figure(s), the reader is referred to the web version of this article.)

decreases towards the surface following a steep plume adiabatic gradient.

3.8. Pulses of activity

The activity of a given mantle plume progressively decreases through time, as evident in the decrease of plume maximum temperature excess from +500 K to +200 K for a hotspot in Model 2 (Fig. 2d). This cooling is consistent with geological estimates of the temperature evolution of the Galapagos and Iceland plumes (Herzberg and Gazel, 2009). The long-term decrease of the activity of a plume is punctuated by shorter-term fluctuations in flux by about $\pm 1 \times 10^3 \text{ kg s}^{-1}$ on 5–10 Myr timescales. Changes in plume buoyancy flux tend to occur after plume merging events or after interaction with a ridge (Fig. 2d).

3.9. Absolute motions of plumes

In Model 1 (stagnant lid), the average absolute drift of plumes in the upper mantle is 0.6 cm yr^{-1} . In contrast, the average absolute lateral speed of upper mantle plumes is approximately 1.8 cm yr^{-1} in Models 2 and 3, 2.2 cm yr^{-1} in Model 4 (more vigorous lower mantle convection), and 2.4 cm yr^{-1} in Model 5 (deep thermochemical piles), which is characterised by more slowly ris-

ing plumes (Table 2). Average absolute lateral speeds of plume conduits in the lower mantle are 15 to 40% lower than in the upper mantle, depending on model parameters; they vary between 0.4 cm yr^{-1} (Model 1) and 2 cm yr^{-1} (Model 5). This reflects that some plumes are tilted by vigorous upper mantle convection.

3.10. Relative motion between plumes

We quantified the evolution of the relative motion of pairs of plumes (Table 2 and Fig. 5) to study the processes controlling plume lateral motion. This allowed us to statistically compare the lateral motions of model plumes with observations without considering the global reference frame of tectonic reconstructions. The average relative speed between mantle plumes in the upper mantle is 0.6 cm yr^{-1} in Model 1, 1.6 cm yr^{-1} in Models 2 and 3, and 2.2 cm yr^{-1} in Models 4 and 5. Relative velocities between mantle plumes are systematically lower than the average absolute motion of plumes in models with a plate-like tectonic behaviour, which suggests a coherent drift of at least some mantle plumes (see section 4.2). However, in these models, the net motion of the mantle relative to the surface has a small effect on plume lateral motion because it is only about $0.03\text{--}0.04^\circ \text{ Myr}^{-1}$ (Table 2), at the low end of net rotation estimates (Tetley et al., 2019).

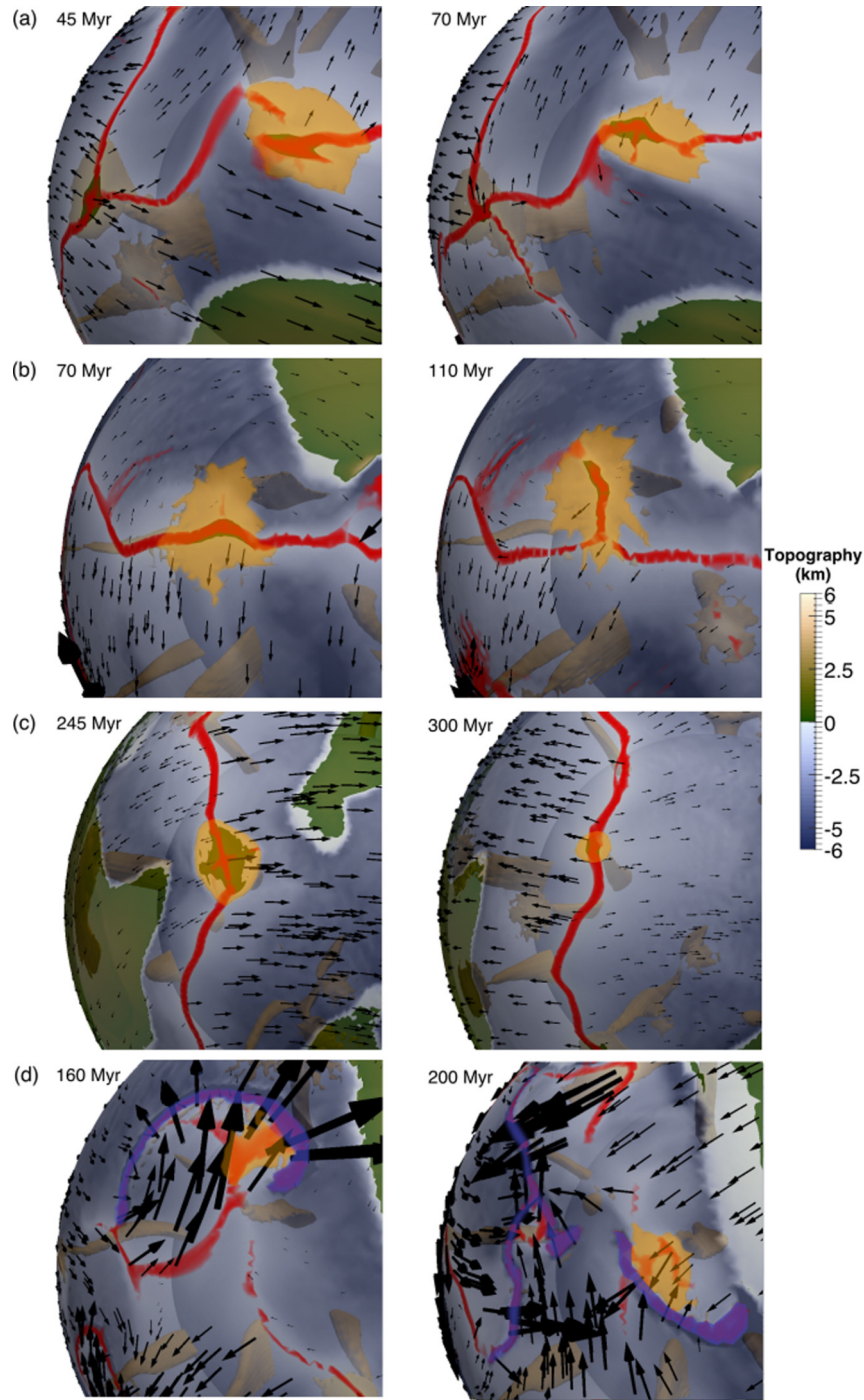


Fig. 6. Four cases of ridge-plume interactions in Model 2: (a) plume ponding below a stable ridge (b) ridge-jump in the vicinity of a plume, (c) ridge-propagation induced by a plume, and (d) backarc-plume interaction. Surface topography is outlined as a transparent field. Arrows represent surface velocities. Plume isotherms are seen by transparency in blue. The thermal trail of considered plumes are highlighted in brighter orange. Ridges are in red and subduction zones are in transparent orange. The camera is fixed for each temporal evolution. (For interpretation of the colours in the figure(s), the reader is referred to the web version of this article.)

More than 76% of model plumes move by less than 2 cm yr^{-1} depending on model parameters (Fig. 5a). This is comparable to results from Li and Zhong (2019), after the removal of the net motion of the mantle from their modelled plume motions; in their models, large mantle net rotation results from both imposed surface boundary conditions containing net-rotation up to $0.55^\circ \text{ Myr}^{-1}$, and stronger viscous coupling between the lithosphere and asthenosphere.

Dobrovine et al. (2012) produced a global moving hotspot reference frame from the best fit of advected tracers within a recon-

structed mantle flow during the last 130 Ma with the tracks of 44 well-known hotspots. They found that limited plume motion (drift of less than 3 cm yr^{-1} for any plume, Fig. 5a) and large plume deflection could explain observed hotspot tracks. This scenario requires plumes to drift slower than in Models 2-5. However, this reference frame results in large lithospheric net rotation (Table 2), and it neglects potential large uncertainties on both hotspot track ages and paleo-locations, as well as uncertainties in backward-advection mantle flow models. To overcome the limitations associated with the use of uncertain paleomagnetic estimates and

incomplete geological record, Tetley et al. (2019) generated an absolute plate motion model assuming fixed hotspots and optimising trench motion, lithospheric net rotation and hotspot track geometry. From the difference between nine modelled and observed hotspot tracks, they estimated relative mantle plume motions as $2.07 \pm 0.8 \text{ cm yr}^{-1}$, which is 85% larger than Doubrovine et al. (2012). Our results are compatible with that of Tetley et al. (2019) (Fig. 5a and Table 2).

3.11. Topographic swell

In all models, the buoyancy force of mantle plumes leads to the formation of a surface topographic swell 1000–2000 km across and 1–2 km high (Fig. 1, S3 and S5). The swell extent and amplitude depend on 1/ plume buoyancy flux that decreases over time (Fig. 2 and Movies S1 and S2), 2/ the nature of the impacted lithosphere (thickness, type, plate boundary proximity) and 3/ the relative motion between the plume and the lithosphere, which can shear the conduit and result in an asymmetric shape of the plume trail (Fig. S2, Movies S1 and S2; see also Arnould et al., 2019).

3.12. Plume-ridge interactions

In Models 2–4, 30 to 50% of mantle plumes interact with ridges at one point (Fig. 2c). This proportion increases to 45–80% for Model 5 in which the weaker lithosphere is more likely to break above mantle plumes. The increasing number of plumes interacting with ridges during the last 150 Myr in Model 5 represents a rise of total ridge length during a significant rifting event, with the newly formed ridges connecting over preexisting mantle plumes (Coltice et al., 2019). This preferential relation between ridges and mantle plumes was first noted by Wilson (1965).

Some model plumes interacting with ridges are relatively stable ($<2 \text{ cm yr}^{-1}$) and stay in the vicinity of a long-lived ridge for at least 50 Myr (Fig. 6a). This case represents the proposed long-term interactions between the Mid-Atlantic ridge and Tristan, St-Helena and the Azores (e.g. Gente et al., 2003). Plumes moving along or near a ridge can favour ridge-jumps (Fig. 6b), in a configuration comparable to the interaction of the Nazca ridge with the Galapagos hotspot (Wilson and Hey, 1995). Such jumps can also occur when a plume reaches the surface in the vicinity of an existing ridge, resulting in the relocation of the ridge axis above the newly-formed hotspot. This phenomenon has been invoked for the formation of the Elan bank during the emplacement of the Kerguelen plateau and in the Tasman Sea (Gaina et al., 2003), although paleomagnetic measurements in these regions are debated (Sandwell and Smith, 1997). This mechanism possibly explains why slowly-migrating ridges often interact with plumes (Whittaker et al., 2015). Finally, some plumes can cross ridge axes and contribute to the propagation of a new spreading axis (Fig. 6c). This case shares similarities with the Réunion hotspot crossing the Central Indian Ridge about 30 Myr ago and its putative link to the formation of the Rodriguez ridge (Morgan, 1978).

4. Sources of plume drift

We used the above analysis of the characteristics of model plumes to classify the lateral plume motions into categories. We used Model 1 as a reference to define four categories reflecting four different processes.

4.1. “Fixed” plumes

In Model 1, 60% of plumes move by less than 0.5 cm yr^{-1} relatively to each other (Fig. 5a). These plumes are rooted at saddle points of basal flow and therefore remain stable throughout their

lifetime. This stability is favoured by the absence of plate tectonics at the surface, since the number of fixed plumes decreases to between 25% (Model 5) and 50% (Model 3) when plate-like behaviour occurs (Fig. 5a). The most stable plumes are still located at saddle points of lowermost mantle flow (such as Plume IDs 1, 4, 7, 16 and 21 on Fig. S9), which is consistent with the numerical models of Zhong et al. (2000). In Li and Zhong (2019), the proportion of fixed plumes is 10–20%, possibly due to the deep mantle rotation induced by imposed plate velocities (Rudolph and Zhong, 2014).

4.2. Basal mantle flow entrainment

In Model 1, about 30% of model plumes move at relative speeds comprised between 0.5 and 1 cm yr^{-1} (Fig. 5a). Such lateral speeds are consistent with average lower mantle lateral motions (Table 2), suggesting entrainment of these plumes by lateral flow in the lowermost mantle. In Models 2–5, the number of slowly-moving plumes varies from 25% of the total number of plumes (Model 4) to 40% (Model 2). The lateral motion of such plumes (e.g. IDs 18 and 18) coincides in direction and magnitude with the lowermost mantle flow in their vicinity (Fig. 5a and Table 2).

4.3. Slab-induced drift

This category of plumes drifting at speeds between 1 – 5 cm yr^{-1} over several tens of million years only occurs with plate-like behaviour (Models 2–5) and is indirectly related to subduction dynamics. 28% (Model 2) to 40% (Model 5) of model plumes belong to this category (Fig. 5). In these models, slabs penetrating in the lower mantle as far as 5,000 km away from mantle plumes modify the mantle pressure field by generating regional positive pressure gradients in the basal thermal boundary layer (Fig. 7a) resulting in plume motions at about 2 cm yr^{-1} . Some close conduits can therefore be pushed in a similar direction by these regional reorganisations of mantle flow, such as Plume ID 6, 10 and 15 in Model 2 (Fig. S9). Faster lateral motions result from complex interactions between plume conduits (which are subsequently highly deformed) and slabs in the upper mantle and the uppermost lower mantle (Movies S1, S2 and S3). In Model 5, slabs also contribute to deforming the edges of thermochemical heterogeneities and therefore indirectly push mantle plumes. This process is consistent with the scenario proposed by Hassan et al. (2016) to explain the fast ($>4 \text{ cm yr}^{-1}$) drift of the Hawaii plume between 81 and 47 Ma.

4.4. Rapid drift due to plume merging events

Independent of the presence of surface plate-like motions, all models feature plumes with lateral speeds exceeding 5 cm yr^{-1} and reaching 10 cm yr^{-1} (Model 1) to 22 cm yr^{-1} (Models 2 and 4). Less than 5% of all mantle plumes drift at such speeds which occur when two mantle plumes, whose roots are within a few hundreds of kilometres of one another, merge (Fig. 7b). Plume merging events have a recurrence time varying between 35 Myr (Models 3 and 5) and 200 Myr (Models 1 and 2). Merging between two mantle plumes always starts at the base of the mantle due to a basal pressure difference between two close conduits, and propagates to the upper mantle, where the last merging steps occur over less than 10 Myr (Fig. 5b and Fig. 7b). Merging between two mantle plumes has been described in mantle convection models (Davies and Davies, 2009), but fast lateral motions of merging mantle plumes have not yet been documented on Earth, which could be explained by the rare occurrence and short duration of such model events.

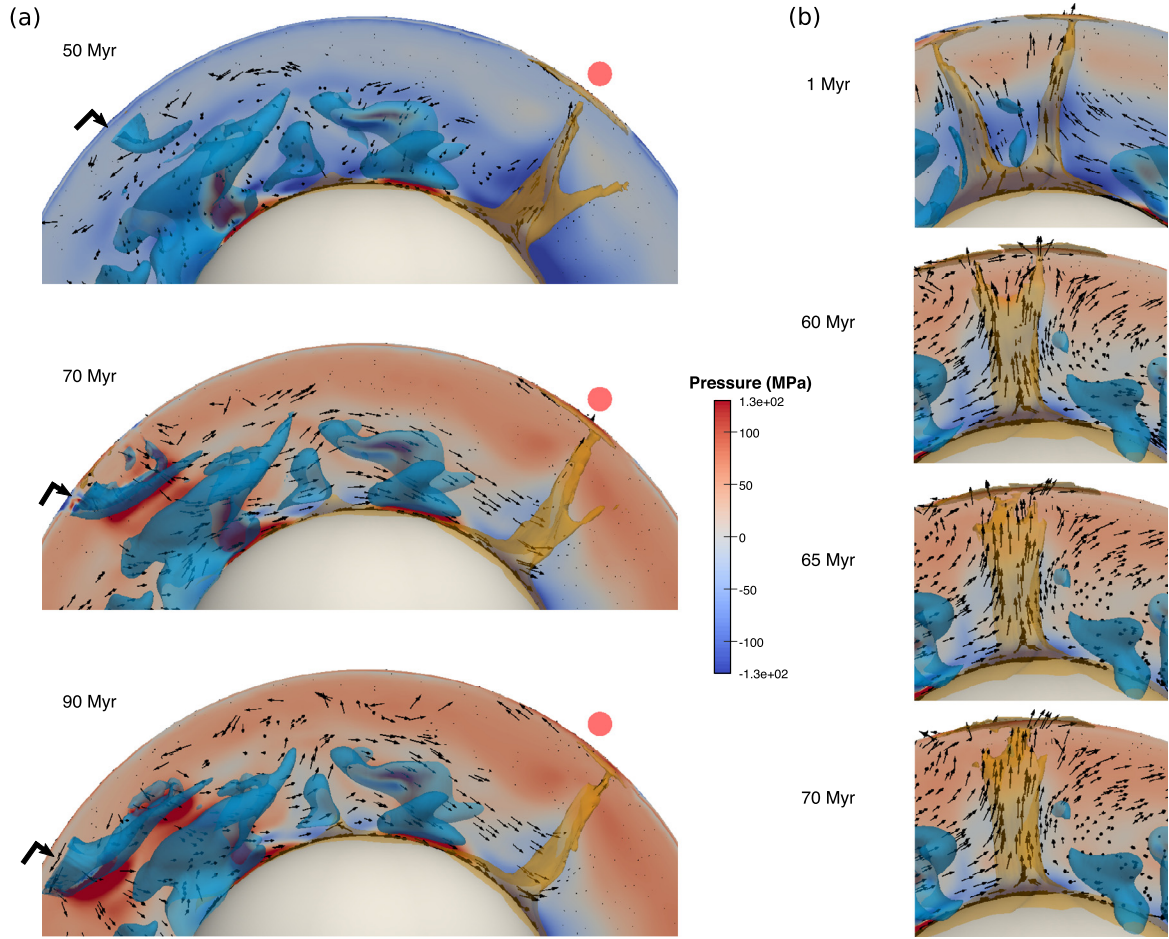


Fig. 7. Examples of pressure-gradient-induced plume drifts in Model 2. Mantle plumes are highlighted by orange transparent isotherms and subducting lithosphere is shown as transparent blue isotherms. The velocity field is shown as black arrows. In (a), the position of the plume is indicated at each timestep with a red circle. Subduction (the thick black arrow shows the location of the trench) initiates on the left-hand-side, which results in far-field compression and horizontal lower mantle flow directed towards the plume. (b) Merging of two mantle plumes starting from the base of the mantle and propagating upwards. The camera is fixed. (For interpretation of the colours in the figure(s), the reader is referred to the web version of this article.)

5. Discussion

5.1. Limitations of models and analysis

We tested a limited number of parameters potentially affecting plume drift. For example, we only considered one parameterisation (initial thickness, density and viscosity contrasts) to model basal thermochemical heterogeneities, although the nature of LLSVPs remains debated (e.g. Garnero et al., 2016). Moreover, although the resolution at 350 km depth in Models 2–4 (33 km) is lower than the one of Models 1 and 5 (24 km, similar to the lateral resolution of Li and Zhong (2019)), the ranges of detected cross-sectional areas for all models are consistent (Fig. 3a). Furthermore, we achieved radial and lateral viscosity contrasts as large as 10^7 Pa s at the expense of model computational time: each model required about 145,000 CPU hours over three months of calculation on a parallel supercomputer to model mantle flow over 350 Myr.

Our plume detection algorithm is based on the hypothesis that all mantle plumes are characterised by significant heat advection, and therefore by both substantial temperatures and large rising speeds. This method makes it possible to characterise model plume dynamics, however results depend on 1/ the ability to detect a potentially large variety of plumes in models with distinct parameters, and 2/ on the threshold that is set for plume detection. This threshold was defined by comparing the number of plumes de-

tected by the algorithm to the number of mantle plumes detected visually.

5.2. What controls plume dynamics?

Here, we focus on the causes of lateral motions of already developed plumes and do not investigate the controls on the position of their source, which is likely to also affect their dynamics (e.g. Heyn et al., 2018; Li and Zhong, 2017).

5.2.1. Indirect control by plate tectonics

Despite these limitations, we show that planetary surface dynamics exerts a first-order control on plume drift: if the surface is in stagnant lid, stable or slowly moving plumes predominate. The impossibility for mantle plumes to drift rapidly in the absence of plate tectonics and lithospheric thickness heterogeneities was noted by Zhong (2009) who studied the origin of Martian volcanism. Plate-like behaviour promotes faster plume motion (Fig. 5) due to the interaction of plume conduits with slabs in the upper or the lower mantle. Nevertheless, we see no significant effect of the number of plates (comparison between Model 2 and 3) on the statistical distribution of lateral plume motions.

5.2.2. Limited stabilisation of mantle plumes by mid-ocean ridges

It has been proposed that mantle plumes can be pinned to stable ridges (Tarduno et al., 2009). In our models, three plume

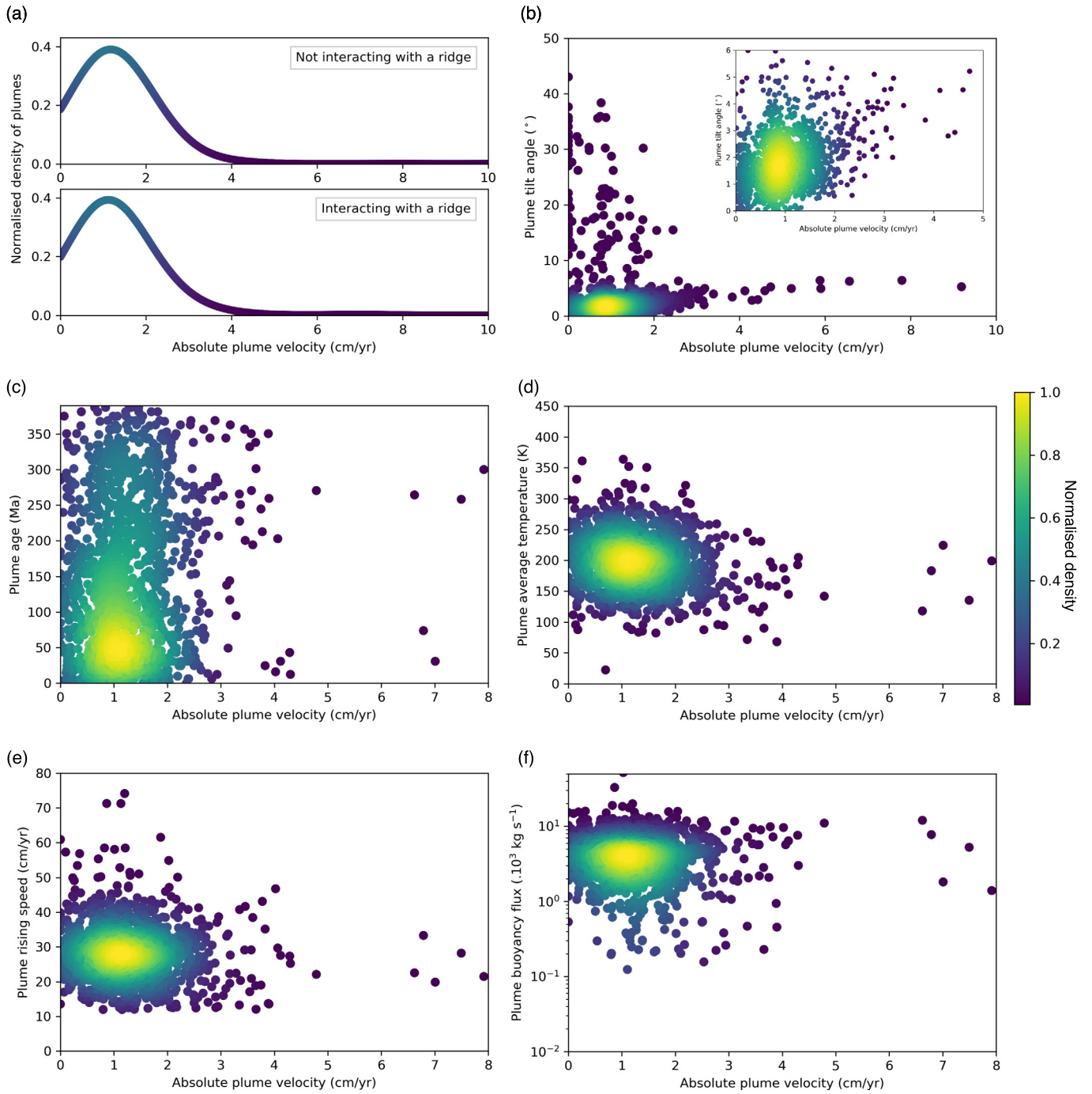


Fig. 8. Distribution of (a) plumes interacting (bottom panel) or not (top panel) with ridges, (b) plume tilt angle between 150 and 670 km depth, (c) plume age, (d) plume temperature excess, (e) plume rising speed and (f) plume buoyancy flux versus plume absolute velocity for Model 2. The colour scale shows the normalised density of mantle plumes on each plot. The inset on (b) shows a closeup view on the largest density of plumes of that plot.

behaviours arise depending on the type of spreading centre they interact with. A limited number of plumes pond below and remain fixed to long and stable ridges (e.g. Hotspot 7 in Fig. S9, from 90 Ma), consistently with Whittaker et al. (2015). In contrast, plumes may move along a stable ridge due to slab-induced lower mantle flow during several tens of million years (Hotspots 10 and 15 of Fig. S9). The possible slow motion of the Azores plume could fall in that category (Arnould et al., 2019). Finally, mantle plumes interacting with fast-migrating ridges, usually neighbouring small plates affected by fast reorganisations, tend to move laterally faster and more erratically (Fig. 6d). We find no statistical difference in

the lateral motion distribution of plumes as a function of their interacting with ridges (Fig. 8a).

5.2.3. The role of the mantle environment on plume dynamics

Lower mantle convection vigour seems to play a limited role in plume drift (comparison between Model 2 and 4) while affecting the number of active plumes. This result is consistent with that of Li and Zhong (2019), who did not detect any change in the statistical distribution of plume lateral motions when changing the Rayleigh number in mantle convection models with imposed plate histories.

We do not observe significant and systematic plume conduit deflection by mantle wind (Fig. 4). The strong temperature-dependence of mantle viscosity causes plume material to rise 10–100 times faster than typical ambient flow in the upper mantle (Fig. 3c). Therefore, plume material rises too quickly to be substantially deflected (Fig. 4b). This conclusion differs from the results of numerical models of mantle convection with imposed plate history (e.g. Steinberger and O'Connell, 1998; O'Neill et al., 2005), which advocate for a strong effect of mantle wind on plume conduit tilting and plume motions to fit hotspot tracks. However, these models do not consider fully-dynamic mantle plumes. Instead, passive tracers are advected within a seismically and tectonically reconstructed mantle flow at a constant rising speed (2.2 cm yr^{-1} in Steinberger and O'Connell (1998) to 10 cm yr^{-1} in Steinberger and Antretter (2006)) and with an assigned maximal tilt angle of 60° , constrained by experimental values on chemical plumes (Whitehead, 1982). We note that our model plumes generate Earth-like buoyancy fluxes, that our findings are consistent with other numerical studies of mantle convection with a free-slip surface (Zhong et al., 2000; Davies and Davies, 2009) and that models with imposed plate history also generate mainly vertical fully-dynamic plumes (Li and Zhong, 2019) as opposed to significantly deflected plumes.

Model mantle plumes rooted at the edges of basal thermochemical heterogeneities tend to be more mobile (Fig. 5a) and are more likely to be deflected (Fig. 4) than purely thermal plumes (Davaille et al., 2002; Li and Zhong, 2019) because the entrainment of dense material by plume conduits slows their rise by a factor of two in our experiments.

5.2.4. Plume characteristics are not diagnostic of plume motions

We assess the relationships between model plume lateral velocities and age (defined as the time since a new plume was first detected), tilt angle, temperature excess, rising speed and buoyancy flux, to explore whether it may be possible to estimate plume drifting rates from such observations for Earth (Fig. 8 and S10). We find that plume age, temperature excess, rising speed and buoyancy flux do not correlate with absolute plume velocity. Moreover, plume tilt angles do not correlate with plume drifting rates (Fig. 8b). Instead, fast-moving plumes are characterized by small tilt angles. This suggests that intrinsic plume characteristics cannot be used as a diagnostic for plume drift.

5.3. Implications for absolute plate reconstructions

The study of the statistical behaviour of mantle plumes is critical to interpret the paleomagnetic and geochronological record and to build absolute plate reference frames based on moving hotspots for the last $\sim 80 \text{ Myr}$. In our study, 25% (Model 5) to 50% (Model 3) of plumes move at $<0.5 \text{ cm yr}^{-1}$ during several tens of millions of years in models with plate tectonics. This significant proportion of slow-moving plumes is comparable to the proportion of stable hotspots of Doubrovine et al. (2012) and Tetley et al. (2019), in which 52% and 30% of Earth plumes move by less than 0.5 cm yr^{-1} , respectively (Fig. 5a), although we note that observations of plume absolute motions are uncertain, notably for motion along the direction of hotspot tracks (Li and Zhong, 2019). We can nevertheless propose that such hotspots can be used as a robust non-moving reference to reconstruct plate motions.

Moreover, our results show that plumes with different drifting rates can coexist within the same global convective system, depending on their location and potential interactions with slabs, plate tectonics and regional convective flow (Fig. S9). Indeed, model plume velocities can exceed 2 cm yr^{-1} , consistent with geochronological and paleomagnetic observations for Hawaii (Tarduno et al., 2003; Konrad et al., 2018) and Kerguelen (Antretter

et al., 2002). Our study therefore reconciles contradictory observations of plume drift and suggests that defining a global reference frame based on hotspot tracks to reconstruct past absolute plate motions requires the careful selection of slow-moving plumes based on paleomagnetic and geochronological data.

6. Conclusion

We presented mantle plumes arising in models of mantle convection self-generating plate-like tectonics that display excess temperatures, rising speed and buoyancy fluxes comparable with Earth's major hotspots. In the absence of plate tectonics, mantle plumes are long-lived, vertical and fixed. In models with plate tectonics, plumes rise vertically with deflection $<10^\circ$ on average, usually limited to the more vigorously convecting upper mantle, consistently with recent tomographic models (French and Romanowicz, 2015). Plume lifetime is shorter with tectonics than in stagnant lid mode, with half of plumes existing for less than 50 Myr, although some plumes may exist for hundreds of million years. The coexistence of several long-lived plumes with short-lived ones is consistent with observations from LIPs (Large Igneous Provinces) and hotspot tracks.

With plate tectonics, plumes are in general mobile. We identified four distinct groups of plumes:

1. 25–50% of plumes are fixed to saddle points of the basal mantle flow. Their velocity is $<0.5 \text{ cm yr}^{-1}$. They can be used as reference to reconstruct absolute plate motions.
2. 25 to 40% of plumes are entrained by passive mantle flow; they move at speeds between $0.5\text{--}1 \text{ cm yr}^{-1}$ without interaction with dynamic instabilities such as slabs or other plumes.
3. 30–40% of plumes are pushed by slabs sinking in the lowermost mantle that generate high pressures in the basal boundary layer, pushing plumes towards lower pressure regions. Such plume motion is between 1 and 5 cm yr^{-1} , can last several tens of million years, and may explain the large speeds of the Hawaiian plume (e.g. Konrad et al., 2018).
4. Rare (once every 200 Myr in some models) merging of close plumes due to a pressure difference in the basal boundary layer. Merging starts in the thermal boundary layer at a slow pace. Plumes drift at speeds $>5 \text{ cm yr}^{-1}$ over less than 10 Myr once merging propagates to the upper mantle.

The limited deflection of plume conduits results from their strong temperature dependence of viscosity. The entrainment of basal thermochemical material by mantle plumes decreases their buoyant rising speed, leading to enhanced plume deflection, lateral plume motion and shorter lifetime.

Our models suggest that ridges are passive enough to interact with plumes but not to systematically influence the flow where plumes originate. Some plumes leave ridge segments, other move along with a fast-drifting ridge, and some move along a stable ridge axis.

The intrinsic properties of plumes observed from the surface (age, excess temperature, buoyancy flux, rising speed, tilt angle) are not diagnostic of plume motion since they do not correlate with lateral plume velocity.

Data availability

Data available in data repository Open Science Framework at: <https://osf.io/up7df/>.

Declaration of competing interest

The authors declare that they have no known competing financial interests or personal relationships that could have appeared to influence the work reported in this paper.

Acknowledgements

The research leading to these results received funding from the European Research Council within the framework of the SP2-Ideas Program ERC-2013-CoG, under ERC grant agreement 617588. N.F. was supported by ARC grants DE160101020 and LP170100863 and C.M. was supported by ARC grant IH130200012. The models were generated with the code StagYY which is the property of P.J. Tackley and ETH-Zürich. It is available for collaborative studies from P.J. Tackley (paul.tackley@erdw.ethz.ch). We provide the minor modifications of the code StagYY, which are specific to this study upon request. This research benefited from the assistance of resources from the National Computational Infrastructure (NCI), which is supported by the Australian Government. We thank S. Zhong and K. Konrad for their constructive reviews that improved this article.

Appendix A. Supplementary material

Supplementary material related to this article can be found online at <https://doi.org/10.1016/j.epsl.2020.116439>.

References

- Allmann, B.P., Scheerer, P.M., 2009. Global variations of stress drop for moderate to large earthquakes. *J. Geophys. Res.* 114.
- Antretter, M., Steinberger, B., Heider, F., Soffel, H., 2002. Paleolatitudes of the Kerguelen hotspot: new paleomagnetic results and dynamic modeling. *Earth Planet. Sci. Lett.* 202, 635–650.
- Arnould, M., Coltice, N., Flament, N., Seigneur, V., Muller, R.D., 2018. On the scales of dynamic topography in whole-mantle convection models. *Geochem. Geophys. Geosyst.* 19, 3140–3163.
- Arnould, M., Ganne, J.N.C., Feng, X., 2019. Northward drift of the Azores plume in the earth's mantle. *Nat. Commun.* 10.
- Brace, W., Kohlstedt, D., 1980. Limits on lithospheric stress imposed by laboratory experiments. *J. Geophys. Res.* 85, 6248–6252.
- Bunge, H.P., 2005. Low plume excess temperature and high core heat flux inferred from non-adiabatic geotherms in internally heated mantle circulation models. *Phys. Earth Planet. Inter.* 153, 3–10.
- Chopelas, A., Boehler, R., 1992. Thermal expansivity in the lower mantle. *Geophys. Res. Lett.* 19, 1983–1986. <https://doi.org/10.1029/92GL02144>.
- Coltice, N., Gerault, M., Ulvrova, M., 2017. A mantle convection perspective on global tectonics. *Earth-Sci. Rev.* 165, 120–150.
- Coltice, N., Husson, L., Faccenna, C., Arnould, M., 2019. What drives tectonic plates? *Sci. Adv.* 5.
- Courtillot, V., Davaille, A., Besse, J., Stock, J., 2003. Three distinct types of hotspots in the earth's mantle. *Earth Planet. Sci. Lett.* 205, 295–308.
- Cramer, F., Tackley, P., Meilick, I., Gerya, T., Kaus, B., 2012. A free plate surface and weak oceanic crust produce single-sided subduction on earth. *Geophys. Res. Lett.* 39. <https://doi.org/10.1029/2011GL050046>.
- Crosby, A., McKenzie, D., 2009. An analysis of young ocean depth, gravity and global residual topography. *Geophys. J. Int.* 178, 1198–1219.
- Davaille, A., Carrez, P., Cordier, P., 2018. Fat plumes may reflect the complex rheology of the lower mantle. *Geophys. Res. Lett.* 45, 1349–1354.
- Davaille, A., Girard, F., Le Bars, M., 2002. How to anchor hotspots in a convecting mantle? *Earth Planet. Sci. Lett.* 203, 621–634.
- Davaille, A., Vatteville, J., 2005. On the transient nature of mantle plumes. *Geophys. Res. Lett.* 32.
- Davies, D.R., Davies, J.H., 2009. Thermally-driven mantle plumes reconcile multiple hot-spot observations. *Earth Planet. Sci. Lett.* 278, 50–54.
- Davies, G.F., 1988. Ocean bathymetry and mantle convection, 1: large-scale flow and hotspots. *J. Geophys. Res., Solid Earth* 93, 10467–10480.
- Dobrovine, P.V., Steinberger, B., Torsvik, T.H., 2012. Absolute plate motions in a reference frame defined by moving hot spots in the Pacific, Atlantic, and Indian oceans. *J. Geophys. Res., Solid Earth* 117.
- Duncan, R., 1981. Hotspots in the southern oceans—an absolute frame of reference for motion of the Gondwana continents. *Tectonophysics* 74, 29–42.
- Duncan, R., 1984. Age progressive volcanism in the new england seamounts and the opening of the central Atlantic ocean. *J. Geophys. Res.* 89, 9980–9990.
- Duncan, R.A., Richards, M.A., 1991. Hotspots, mantle plumes, flood basalts, and true polar wander. *Rev. Geophys.* 29, 31–50.
- Finlayson, V., Konter, J., Konrad, K., Koppers, A., Jackson, M., Rooney, T., 2018. Sr–Pb–Nd–Hf isotopes and $^{40}\text{Ar}/^{39}\text{Ar}$ ages reveal a Hawaii–Emperor-style bend in the Rurutu hotspot. *Earth Planet. Sci. Lett.* 500, 168–179.
- French, S.W., Romanowicz, B., 2015. Broad plumes rooted at the base of the earth's mantle beneath major hotspots. *Nature* 525, 95.
- Gaina, C., Muller, R., Brown, B., Ishihara, T., 2003. Microcontinent formation around Australia. In: *Special Papers – Geological Society of America*, pp. 405–416.
- Garnero, E.J., McNamara, A.K., 2008. Structure and dynamics of earth's lower mantle. *Science* 320, 626–628.
- Garnero, E.J., McNamara, A.K., Shim, S.H., 2016. Continent-sized anomalous zones with low seismic velocity at the base of earth's mantle. *Nat. Geosci.* 9, 481.
- Gente, M., Dymant, J., Marcia, M., Goslin, J., 2003. Interaction between the mid-Atlantic ridge and the Azores hot spot during the last 85 myr: emplacement and rifting of the hot spot-derived plateaus. *Geochem. Geophys. Geosyst.* 4.
- Hassan, R., Flament, N., Gurnis, M., Bower, D.J., Müller, D., 2015. Provenance of plumes in global convection models. *Geochem. Geophys. Geosyst.* 16, 1465–1489.
- Hassan, R., Müller, R.D., Gurnis, M., Williams, S.E., Flament, N., 2016. A rapid burst in hotspot motion through the interaction of tectonics and deep mantle flow. *Nature* 533, 239–242.
- Herzberg, C., Gazel, E., 2009. Petrological evidence for secular cooling in mantle plumes. *Nature* 458, 619.
- Heyn, B.H., Conrad, C.P., Tronnes, R.G., 2018. Stabilizing effect of compositional viscosity contrasts on thermochemical piles. *Geophys. Res. Lett.* 45, 7523–7532.
- Jellinek, A.M., Manga, M., 2004. Links between long-lived hot spots, mantle plumes, d", and plate tectonics. *Rev. Geophys.* 42.
- Koivisto, E.A., Andrews, D.L., Gordon, R.G., 2014. Tests of fixity of the Indo-Atlantic hot spots relative to Pacific hot spots. *J. Geophys. Res., Solid Earth* 119, 661–675.
- Konrad, K., Koppers, A.A., Steinberger, B., Finlayson, V.A., Konter, J.G., Jackson, M.G., 2018. On the relative motions of long-lived Pacific mantle plumes. *Nat. Commun.* 9, 854.
- Konter, J.G., Hanan, B.B., Blichert-Toft, J., Koppers, A.A., Plank, T., Staudigel, H., 2008. One hundred million years of mantle geochemical history suggest the retreating of mantle plumes is premature. *Earth Planet. Sci. Lett.* 275, 285–295.
- Labrosse, S., 2002. Hotspots, mantle plumes and core heat loss. *Earth Planet. Sci. Lett.* 199, 147–156.
- Lay, T., Hernlund, J., Buffett, B., 2008. Core–mantle boundary heat flow. *Nat. Geosci.* 1, 25–32.
- Leng, W., Gurnis, M., 2012. Shape of thermal plumes in a compressible mantle with depth-dependent viscosity. *Geophys. Res. Lett.* 39.
- Leng, W., Zhong, S., 2008. Controls on plume heat flux and plume excess temperature. *J. Geophys. Res., Solid Earth* 113.
- Li, M., Zhong, S., 2017. The source location of mantle plumes from 3d spherical models of mantle convection. *Earth Planet. Sci. Lett.* 478, 47–57.
- Li, M., Zhong, S., 2019. Lateral motion of mantle plumes in 3d geodynamic models. *Geophys. Res. Lett.* 46, 4685–4693.
- Mittelstaedt, E., Tackley, P.J., 2006. Plume heat flow is much lower than CMB heat flow. *Earth Planet. Sci. Lett.* 241, 202–210. <https://doi.org/10.1016/j.epsl.2005.10.012>.
- Montelli, R., Nolet, G., Dahlen, F., Masters, G., 2006. A catalogue of deep mantle plumes: new results from finite-frequency tomography. *Geochem. Geophys. Geosyst.* 7.
- Morgan, J., 1978. Rodriguez, Darwin, Amsterdam, ... a second type of hotspot Island. *J. Geophys. Res.* 83, 5355–5360.
- Morgan, W.J., 1972. Plate motions and deep mantle convection. *Geol. Soc. Am. Mem.* 132, 7–22.
- Morgan, W.J., 1981. 13. Hotspot tracks and the opening of the Atlantic and Indian oceans. *The Oceanic Lithosphere*, vol. 7, p. 443.
- Muller, R., Cannon, J., Qin, X., Watson, R., Gurnis, M., Williams, S., Pfaffmoser, T., Seton, M., Russell, S., Zahirovic, S., 2018. GPlates: building a virtual earth through deep time. *Geochem. Geophys. Geosyst.* 19, 2243–2261.
- Nakiboglu, S., Lambeck, K., 1980. Deglaciation effects on the rotation of the earth. *Geophys. J. Int.* 62, 49–58. <https://doi.org/10.1111/j.1365-246X.1980.tb04843.x>.
- O'Neill, C., Müller, D., Steinberger, B., 2005. On the uncertainties in hot spot reconstructions and the significance of moving hot spot reference frames. *Geochem. Geophys. Geosyst.* 6.
- Parnell-Turner, R., White, N., Henstock, T., Murton, B., MacLennan, J., Jones, S.M., 2014. A continuous 55-million-year record of transient mantle plume activity beneath Iceland. *Nat. Geosci.* 7, 914.
- Poore, H., White, N., Jones, S., 2009. A Neogene chronology of Iceland plume activity from y-shaped ridges. *Earth Planet. Sci. Lett.* 283, 1–13.
- Portnyagin, M., Savelyev, D., Hoernle, K., Hauff, F., Garbe-Schonberg, D., 2008. Mid-cretaceous Hawaiian tholeiites preserved in Kamchatka. *Geology* 36, 903–906.
- Putirka, K.D., 2005. Mantle potential temperatures at Hawaii, Iceland, and the mid-ocean ridge system, as inferred from olivine phenocrysts: evidence for thermally driven mantle plumes. *Geochem. Geophys. Geosyst.* 6.

- Ricard, Y., Richards, M., Lithgow-Bertelloni, C., Le Stunff, Y., 1993. A geodynamic model of mantle density heterogeneity. *J. Geophys. Res., Solid Earth* 98, 21895–21909. <https://doi.org/10.1029/93JB02216>.
- Richards, M.A., 1991. Hotspots and the case for a high viscosity lower mantle. In: *Glacial Isostasy, Sea-Level and Mantle Rheology*. Springer, pp. 571–587.
- Richards, M.A., Griffiths, R.W., 1988. Deflection of plumes by mantle shear flow: experimental results and a simple theory. *Geophys. J. Int.* 94, 367–376.
- Rudolph, M.L., Lekić, V., Lithgow-Bertelloni, C., 2015. Viscosity jump in earth's mid-mantle. *Science* 350, 1349–1352.
- Rudolph, M.L., Zhong, S.J., 2014. History and dynamics of net rotation of the mantle and lithosphere. *Geochem. Geophys. Geosyst.* 15, 3645–3657.
- Sandwell, D.T., Smith, W.H., 1997. Marine gravity anomaly from GEOSAT and ERS 1 satellite altimetry. *J. Geophys. Res., Solid Earth* 102, 10039–10054.
- Sleep, N.H., 1990. Hotspots and mantle plumes: some phenomenology. *J. Geophys. Res., Solid Earth* 95, 6715–6736.
- Steinberger, B., Antretter, M., 2006. Conduit diameter and buoyant rising speed of mantle plumes: implications for the motion of hot spots and shape of plume conduits. *Geochem. Geophys. Geosyst.* 7.
- Steinberger, B., Calderwood, A.R., 2006. Models of large-scale viscous flow in the earth's mantle with constraints from mineral physics and surface observations. *Geophys. J. Int.* 167, 1461–1481.
- Steinberger, B., O'Connell, R.J., 1998. Advection of plumes in mantle flow: implications for hotspot motion, mantle viscosity and plume distribution. *Geophys. J. Int.* 132, 412–434.
- Steinberger, B., O'Connell, R.J., 2000. Effects of mantle flow on hotspot motion. In: *The History and Dynamics of Global Plate Motions*, pp. 377–398.
- Tackley, P., 2008. Modelling compressible mantle convection with large viscosity contrasts in a three-dimensional spherical shell using the yin-yang grid. *Phys. Earth Planet. Inter.* 171, 7–18.
- Tackley, P.J., 1998. Self-consistent generation of tectonic plates in three-dimensional mantle convection. *Earth Planet. Sci. Lett.* 157, 9–22.
- Tackley, P.J., 2000. Self-consistent generation of tectonic plates in time-dependent, three-dimensional mantle convection simulations. *Geochem. Geophys. Geosyst.* 1.
- Tackley, P.J., King, S.D., 2003. Testing the tracer ratio method for modeling active compositional fields in mantle convection simulations. *Geochem. Geophys. Geosyst.* 4. <https://doi.org/10.1029/2001GC000214>.
- Tarduno, J., Bunge, H.P., Sleep, N., Hansen, U., 2009. The bent Hawaiian-Emperor hotspot track: inheriting the mantle wind. *Science* 324, 50–53.
- Tarduno, J.A., Duncan, R.A., Scholl, D.W., Cottrell, R.D., Steinberger, B., Thordarson, T., Kerr, B.C., Neal, C.R., Frey, F.A., Torii, M., et al., 2003. The Emperor Seamounts: southward motion of the Hawaiian hotspot plume in earth's mantle. *Science* 301, 1064–1069.
- Tetley, M., Williams, S., Gurnis, M., Flament, N., Müller, D., 2019. Constraining absolute plate motions since the Triassic. *J. Geophys. Res., Solid Earth*. <https://doi.org/10.1029/2019JB017442>.
- Torsvik, T.H., Doubrovine, P.V., Steinberger, B., Gaina, C., Spakman, W., Domeier, M., 2017. Pacific plate motion change caused the Hawaiian-Emperor bend. *Nat. Commun.* 8, 15660.
- Turcotte, D., Schubert, G., 2014. *Geodynamics*. Cambridge University Press.
- Wang, S., Yu, H., Zhang, Q., Zhao, Y., 2018. Absolute plate motions relative to deep mantle plumes. *Earth Planet. Sci. Lett.* 490, 88–99.
- Whitehead, J.A., 1982. Instabilities of fluid conduits in a flowing earth—are plates lubricated by the asthenosphere? *Geophys. J. Int.* 70, 415–433.
- Whittaker, J., Afonso, J., Masterton, S., Müller, R., Wessel, P., Williams, S., Seton, M., 2015. Long-term interaction between mid-ocean ridges and mantle plumes. *Nat. Geosci.* 8, 479–483.
- Williams, S., Flament, N., Muller, R., Butterworth, N., 2015. Absolute plate motions since 130 ma constrained by subduction zone kinematics. *Earth Planet. Sci. Lett.* 418, 66–77.
- Wilson, D.S., Hey, R.N., 1995. History of rift propagation and magnetization intensity for the Cocos-Nazca spreading center. *J. Geophys. Res., Solid Earth* 100, 10041–10056. <https://doi.org/10.1029/95JB00762>.
- Wilson, J.T., 1963. A possible origin of the Hawaiian Islands. *Can. J. Phys.* 41, 863–870.
- Wilson, J.T., 1965. Evidence from ocean islands suggesting movement in the earth. *Philos. Trans. R. Soc. Lond. A* 258, 45–165.
- Zhong, S., 2006. Constraints on thermochemical convection of the mantle from plume heat flux, plume excess temperature, and upper mantle temperature. *J. Geophys. Res., Solid Earth* 111.
- Zhong, S., 2009. Migration of Tharsis volcanism on Mars caused by differential rotation of the lithosphere. *Nat. Geosci.* 2, 19.
- Zhong, S., Zhang, N., Li, Z.X., Roberts, J.H., 2007. Supercontinent cycles, true polar wander, and very long-wavelength mantle convection. *Earth Planet. Sci. Lett.* 261, 551–564.
- Zhong, S., Zuber, M.T., Moresi, L., Gurnis, M., 2000. Role of temperature-dependent viscosity and surface plates in spherical shell models of mantle convection. *J. Geophys. Res., Solid Earth* 105, 11063–11082.